PAPER

Ammonolytical conversion of microcrystalline gallium antimonide GaSb to nanocrystalline gallium nitride GaN: thermodynamics *vs.* topochemistry

Mariusz Drygaś,[a] Piotr Jeleń,[b] Mirosław M. Bućko,[b] Zbigniew Olejniczak[c] and Jerzy F. Janik*[a]

Reaction of microcrystalline powders of readily available gallium antimonide GaSb with ammonia gas at elevated temperatures afforded in one step high yields of nanocrystalline powders of the semiconductor, gallium nitride GaN. In particular, temperatures of 900–1000 °C and suitable reaction times of 36–170 hours resulted in complete nitridation in the system. GaN was prepared as a mixture of the major stable hexagonal and the minor metastable cubic polytypes. Formation of the cubic GaN was consistent with topochemistry playing a meaningful role in the ammonolysis of the cubic GaSb substrate. Specific experimental conditions, including variations in the reaction temperature/time and manual grinding or high energy ball milling of the substrate, had a significant impact on the final GaN polytype make-up and average crystallite size, the latter ranging from a few to a few tens of nanometers. Under the applied conditions, all by-products were conveniently removed from the reaction mixture as volatile species, thus affording chemically pure GaN nanopowders of very good quality.

1. Introduction

Gallium nitride GaN has become an indispensable part of modern electronics thanks to its attractive and unique features, which dwell on advantageous semiconducting properties. The wide bandgap of 3.4 eV makes hexagonal GaN suitable for diverse optoelectronic applications, notably including the detection and emission of light in the blue and ultraviolet range. In addition, the nitride's feasibility to form solid solutions with other Group III(13)-nitrides and being doped with suitable carriers/centers creates conditions for effective modifications of the material's all-in-one semiconducting, optical and magnetic properties.

There are numerous methods reported for the synthesis of GaN most of which are concerned with seminal thin films applications in light-emitting devices.[1] Recently, for similar reasons, monocrystalline gallium nitride technologies have also received due attention.[2] It appears, however, that knowledge on the reproducible synthesis methods and unequivocal properties of the nanocrystalline powders of Group III(13) nitrides, including the GaN semiconductor, are not yet satisfactory as exemplified by some reviews.[3] In general terms, the synthesis

methods are based mostly on the reactions of affordable gallium metal or oxygen-bearing gallium compounds with a nitriding agent (*e.g.*, ammonia, nitrogen), whereas more elaborate organometallic gallium precursors are also used.

Some of the authors of this report contributed to developing a few synthesis routes to GaN nanopowders such as the metathesis of gallium halides and lithium nitride,[4] nitriding decomposition of gallium imide[5] and cyclotrigalazane[6] as well as aerosol-assisted ammonolysis of gallium nitrate solutions.[5g–i,7] Regarding our studies, one can stress advantages of the anaerobic gallium imide route that yields in an easily controlled way average crystallite sizes of GaN ranging from one to several tens of nanometers and the aerosol-assisted method that uses the affordable gallium nitrate precursor in a relatively large-scale synthesis of particles with a spherical morphology. However, the gallium imide route is a tedious multi-stage process requiring elaborate equipment/techniques and precautions that are characteristic of anaerobic syntheses. In turn, the aerosol-assisted route is a two-step synthesis, resulting typically in crystallite sizes above 30 nm and suffers from the chance of getting residual oxygen in the product. Actually, there are various shortcomings in all the methods known to us to warrant the economical supply of large quantities of pure and size-controlled nanopowders of GaN. In this regard, the scale-up synthesis aspect has become troublesome for us in the otherwise successful attempts to optimize our high-temperature high-pressure sintering of GaN nanopowders into robust and machinable ceramics.[8] Hence, we learned first-hand that there is

[a]AGH University of Science and Technology, Faculty of Energy and Fuels, al. Mickiewicza 30, 30-059 Krakow, Poland. E-mail: janikj@agh.edu.pl

[b]AGH University of Science and Technology, Faculty of Materials Science and Ceramics, al. Mickiewicza 30, 30-059 Krakow, Poland

[c]Institute of Nuclear Physics, Polish Academy of Sciences, ul. Radzikowskiego 152, 31-342 Krakow, Poland

still a need for an economical and well-controlled method of GaN nanopowder synthesis.

In our initial attempt to accomplish such a goal, we re-examined the reaction of gallium arsenide GaAs with ammonia, which appears to be particularly well suited for the synthesis of the rare GaN cubic polytype, c-GaN.[9] The latter variety has been shown to be made in up to 90% yield in admixture with the GaN hexagonal polytype, h-GaN. It can be noted that thermodynamically c-GaN is a metastable phase, and therefore its predominant formation could be linked to favorable topochemical conditions during the ammonolysis with N for As replacements in the cubic lattice of the GaAs substrate. For instance, topochemical circumstances were invoked in explaining the GaN polytype make-up in the pyrolysis of cyclo-trigallazane.[10] In a summary of our research, the GaAs/NH$_3$ system was proven to efficiently yield gallium nitride nanopowders, however, with enhanced proportions of the cubic polytype. In extending this idea, the related gallium pnictides such as gallium antimonide GaSb and gallium phosphide GaP have been subjected to similar chemistry in our laboratory confirming the general trend and these results will be published elsewhere.

This report describes the synthesis of nanocrystalline GaN *via* ammonolysis of microcrystalline gallium antimonide GaSb. In particular, monocrystalline chunks of GaSb were either manually ground in an agate mortar or milled in a high energy ball mill, followed by pyrolysis under a flow of ammonia for up to 170 hours at temperatures in the 800–1000 °C range. The products encompassed yellow (lower temperatures) to grey-yellow (higher temperatures, longer times) powders that were thoroughly characterized.

2. Experimental

2.1. Synthesis

Post-processing chunks of GaSb of commercial quality were acquired as a waste material from the Institute of Electronic Materials Technology, Warszawa, Poland. The material required grinding, which was accomplished using two different methods. In manual grinding, several grams of the chunks were placed in an agate mortar and ground for approximately 10 minutes to afford a grey powder. For deep grinding by a standard wet high energy ball milling, a few grams of chunks were crashed to sizes below *ca.* 1 mm and placed in a grinding bowl of the FRITSCH Pulverisette 7 planetary ball mill onto which 10 mL of dry xylene was added. Twenty 3 minute intermittent grinding periods were applied at 900 rpm, each separated with a 10 minute break to prevent overheating of bowl's content. After each grinding period, the bowl warmed-up to 50–60 °C, which is well below the boiling point of xylene, 140 °C. Following recovery from the bowl, the sticky paste was evacuated for 1 h to remove the volatiles affording an agglomerated grey precursor powder. A batch of 1 to 2 grams of the powder was placed in an alumina boat and inserted into a continuous ceramic reactor in a tube furnace. Prior to heating, the system was purged with high purity ammonia, 99.999%, 30 minutes, 0.05 L min^{-1}, and such a flow rate was maintained throughout the reaction. A

selected reaction temperature was attained at a heating rate of 5 °C min^{-1}. Preliminary experiments were carried out at 800 and 850 °C to afford the major unconverted GaSb, some elemental Sb and mere traces of GaN. For the reaction at 900 °C, two hold times were used, *i.e.*, 90 and 170 h with only the latter affording complete nitridation in the system utilizing manually ground GaSb. For the reaction at 1000 °C, a 36 h heating accomplished the same goal. An additional single experiment at 1050 °C for 6 h was also proven to be efficient. The reactions were carried out using both the manually ground and ball milled GaSb powders. Upon cooling to room temperature under flowing NH$_3$, each sample was evacuated for 30 minutes to remove the volatiles. The final products were grey-yellow, loosely agglomerated powders.

2.2. Characterization

The particle size distribution of the substrate powders was measured using dynamic light scattering on a Nanosizer-ZS from Malvern Instruments. All the final products were characterized using standard powder XRD analysis (X'Pert Pro Panalytical, Cu K$_\alpha$ source; $2\theta = 10°–110°$). Average crystallite sizes were evaluated from the Scherrer's equation by applying the Rietveld refinement method. For the evaluation, changes in the line profile parameters compared to a standard sample were utilized. The profile parameters depend on the instrument settings used for data collection and on the profile function used for the refinement. In our analysis, the full Voigt function was used to describe the profile of the measured diffraction lines. The total profile width is a convolution of the Gaussian profile part and the Lorentzian profile part, which were combined numerically. In such a method, the full width at half-maximum (fwhm) is only one of several fitted parameters. In a few cases of the patterns containing severely overlapped peaks for different phases, the crystallite sizes were estimated from the strongest low angle peaks. X-ray fluorescence XRF determinations were performed on a PANalytical WDXRF Axios mAX spectrometer equipped with a 4 kW Rh lamp. Solid-state ^{71}Ga MAS NMR spectra of three series of samples were obtained. The first two were acquired on the APOLLO console (Tecmag) at the magnetic field of 7.05 T produced by an 89 mm bore superconducting magnet (Magnex). A Bruker HP-WB high-speed MAS probe equipped with a 4 mm zirconia rotor and KEL-F cap was used to acquire the MAS NMR spectra at a spinning rate of 10 kHz. The resonance frequency was equal to 91.385 MHz and a single 2 μs RF pulse was used, which corresponded to a π/4 flip angle in the liquid. The acquisition delay used in the accumulation was 1 s and the typical number of acquisitions ranged from 1000 to 4000. The third series of samples was measured on a 500 MHz Bruker Avance III spectrometer at 152.48 MHz. The spinning rate of the 3.2 mm MAS probe was equal to 20 kHz. A single 0.5 μs RF pulse was used, which corresponded to a π/4 flip angle in the liquid. The acquisition delay used in accumulation was 5 s and 1000 scans were acquired. In all cases, the frequency scale in ppm was referenced to Ga(NO$_3$)$_3$ (1 M in D$_2$O). All resonance positions were uncorrected for the second-order quadrupolar shift. A comparison of the spectra of

one specific sample (900 °C, 170 h) measured at the two frequencies shows that the second order quadrupolar effects are negligible. FT-IR spectra for KBr pellets were obtained using a Nicolet 380 spectrometer. Micro-Raman analysis was carried out using a HORIBA LabRAM HR spectrometer with 532 nm laser, sample power of 20 mW, accumulation time 10 s with 2 scans and confocal hole 1000 μm with long-focus length. UV-Vis data were collected on a Perkin-Elmer spectrophotometer Lambda 35 equipped with a 50 mm integrating sphere. SEM/EDX data were acquired using a Hitachi Model S-4700 scanning electron microscope.

3. Results and discussion

3.1. Chemistry, topochemistry, and thermodynamics in the system

The chemistry behind the metathetical nitridation of GaSb can be summarized by a simplified reaction, mimicking a related case of the GaAs/NH$_3$ system:[9c]

$$GaSb + NH_3 \rightarrow GaN + \text{``SbH}_3\text{''}$$
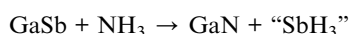
(ΔH_f^0 GaSb = −44 kJ mol^{-1}, ΔH_f^0 NH$_3$ = −46 kJ mol^{-1}, ΔH_f^0 GaN = −157 kJ mol^{-1}), where "SbH$_3$" denotes, in short, all volatile antimony species of an unspecified nature. In this regard, stibine SbH$_3$ itself is a gas that is reported to be unstable under ambient conditions (ΔH_f^0 SbH$_3$ = 145 kJ mol^{-1}) decomposing to antimony Sb and hydrogen H$_2$.[11] For the actual reaction shown below:

$$GaSb + NH_3 \rightarrow GaN + Sb + 3/2H_2$$

the calculated standard reaction enthalpy is ΔH_r^0 = −67 kJ mol^{-1} and therefore, the ammonolysis of GaSb to GaN is thermodynamically favourable.

Bulk elemental Sb has a melting point of 631 °C and a boiling point of 1635 °C. However, nanosized Sb, if formed, would possibly melt at a significantly lower temperature, showing sufficient volatility to be transported in the gas stream out of the reaction zone. In this regard, the partial vapor pressure of Sb at 712 °C, the melting point of GaSb, is *ca.* 10^{-6} atm, which means that during extended reaction times at high temperatures significant quantities of it could be lost/transported out of the reaction vessel.[12] Although the exact mechanism of removing Sb from the system is unknown, the formation of elemental Sb and its persistence in the mixture with GaN, especially, at nitriding temperatures lower than 900 °C and relatively short reaction times was confirmed in this study (*vide infra*). At suitably high temperatures and long hold times, neither GaSb nor Sb were any longer detected by XRD in the product powders. Moreover, all final nanopowders were examined by SEM/EDX and XRF, which showed no Sb within the detection limits of the methods.

It is worth noting that temperatures in the range 800–1000 °C employed here are higher than the melting point of GaSb. This may create a situation wherein surface nitridation with ammonia forms first GaN or transient GaSbN solid layers on otherwise liquid droplets of molten GaSb followed by a different, mostly, diffusion-controlled mechanism of droplets' molten interior nitridation. One may predict, therefore, that the substrate grain size should have a demonstrable effect on the reaction output. However, there was no evidence for bulk melting of the GaSb substrate and the products were loosely agglomerated GaN nanopowders.

Regarding the known chemistry of GaSb with nitrogen sources, available reports mostly describe the formation of GaSbN/GaNSb layers, often, on GaSb substrates *via* various gas or liquid phase-assisted deposition techniques. Such dilute nitride GaSbN/GaNSb structures are known to lead to a reduction in the band gap of GaSb, opening the possibility of using the material for long-wavelength applications. To this end, polycrystalline GaN with elemental Ga were used as the nitrogen source and liquid phase, respectively, to form a GaSbN layer with 1% nitrogen content on a GaSb monocrystal.[13a] Hydrazine solutions were applied to the surface of a GaSb single-crystal wafer to create a postulated GaN monolayer on it.[13b] Dilute nitride GaNSb layers of a few micrometer thickness with up to 1.4% nitrogen were grown on GaSb substrates by MBE using a RF plasma nitrogen source.[13c] A plasma-assisted MBE technique was used to grow dilute GaNSb films at temperatures 310–460 °C with up to 1.7% nitrogen, the latter value being temperature dependent.[13d] A recent review of these efforts, which includes electronic structure calculations in the dilute nitride alloy GaSb$_{1-x}$N$_x$, stresses the complex nature of nitrogen sites, including a single N-incorporation on a Sb site and two nearest-neighbor N centers on the closest Sb sites.[13e] One needs to underline that based on those reports for at least up to *ca.* 1.7% of incorporated N, the GaSbN/GaNSb lattice preserves the cubic symmetry of the GaSb substrate. Moreover, to the best of our knowledge, no reports on the complete nitridation of GaSb and/or reactions of GaSb with NH$_3$ are available to date.

As far as the stability of the GaN polytypes is concerned, theoretical calculations suggest a very small difference in standard total energies between the hexagonal and cubic polytypes.[14] The total energy of cubic GaN (c-GaN) is lower by merely 9.88 meV per atom or 16 meV per unit than that found for hexagonal GaN (h-GaN). These data imply that the formation of the nitride's metastable cubic phase is fundamentally quite probable given the appropriate choice of reaction/experimental conditions (kinetic control, extreme pressure/temperature, substrate surface-nitride layer lattice compatibility, topochemistry). There are quite a few reports confirming the formation of pure c-GaN, mostly, as thin films or polycrystalline products from autoclave syntheses, whereas under moderate conditions the synthesized c-GaN is often accompanied by stable h-GaN either as a mixture of separate bulk phases or defect-related intra-growth of both lattice domains.

In this regard, a very interesting aspect of the GaSb/NH$_3$ system is the potential impact of the topochemical factor on GaN polytype formation. One could envision that under appropriate conditions, the antimony centers in the cubic GaSb would be gradually replaced with nitrogen (from ammonia decomposition) preserving the cubic lattice in the form of transient GaSbN, eventually producing a rare c-GaN. Such a

transitional conversion of c-GaSb to c-GaN *via* a gradual collapse of the cubic lattice is appealing since their *a* lattice constants, 6.1 and 4.5 Å, respectively, differ significantly to otherwise warrant the lattice type preservation. However, if thermodynamics prevail, the stable h-GaN will be formed instead.[15] The latter scenario is likely to take place if molten GaSb reacts with ammonia or if it is preferentially decomposed to its elements and the resulting liquid Ga (mp 30 °C) is then nitrided towards GaN. Therefore, to increase the chances for c-GaN formation, one should minimize the circumstances leading to GaSb melting and/or decomposition, whereas creating conditions for the metathetical N for Sb element replacement *via* nitridation of solid GaSb. From this viewpoint, with other things being equal, the grain size of the powdered GaSb precursor can be one of the key factors impinging the reaction output.

3.2. Discussion of the characterization data

Fig. 1 shows two superimposed particle size distribution curves for the manually ground and ball milled GaSb. It is instructive to compare the two grinding methods and for this the relative dimensions of the black spheres shown under the curves are intended to visualize the size deterioration upon ball milling. In addition, ball milling resulted in a quite symmetrical curve A – some 50% of the particles had diameters $d < 400$ nm and 95% had $d < 600$ nm; practically, the particle sizes covered a narrow range of 200–700 nm. By comparison, the manually ground material showed a broad and asymmetrical curve (curve B) – some 50% of the particles had diameters $d < 12\,000$ nm and 95% had $d < 30\,000$ nm; the particle sizes covered a wide range of 500–50 000 nm. It is clear that there was a significant grain size/grain surface difference between the two batches of precursor.

The representative SEM images of some of the product GaN nanopowders are shown in Fig. 2. Apparently, the particle sizes on the left side (manual grinding) are on average bigger than the ones on the right side (ball milling). It also seems apparent that the particles from the ball milled precursor are more size homogenous. It can be noted that these sizes are not necessarily the crystallite sizes but they rather physically represent
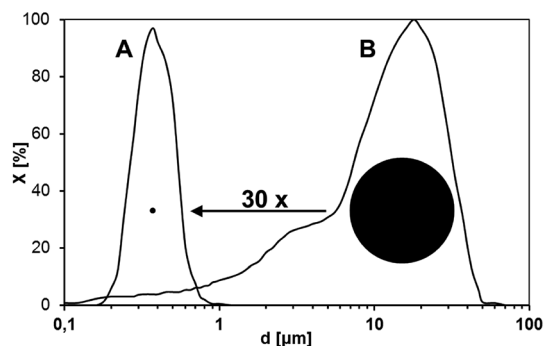

Fig. 1 Particle size distribution of ground GaSb: A – ball milled, B – manually ground. The black spheres visualize a *ca.* 30-fold difference in the average particle diameters.

crystallite agglomerates or mixtures of the two types of particles.[5i] Regarding agglomeration, the materials made from the manually ground GaSb consist mostly of h-GaN and those made from the ball milled GaSb include sizeable proportions of c-GaN (*vide infra*), so the smaller crystallites of c-GaN could have exerted an overall diluting effect on agglomerate formation. However, since the morphological and particle size characteristics of the ground precursor match well those of the respective nitride product (*cf.* Fig. 1 and 2), the essential role of the initial grain size features in the evolution of the nitride product morphology appears to prevail.

A set of reference and representative XRD patterns for the samples prepared from the manually ground and ball milled GaSb, both from nitridation at 900 °C, 170 h, is shown in Fig. 3. The relative amounts and average crystallite sizes of the GaN polytypes for all products, which were estimated from the XRD patterns are included in Table 1.

Utilization of lower reaction temperatures than 900 °C, *e.g.*, 800 and 850 °C, even with reasonably extended reaction times did not succeed in the complete conversion of GaSb and both unreacted GaSb and elemental Sb were detected in addition to GaN. Starting at 900 °C and sufficiently long times, *e.g.*, 170 h for manually ground and 90 h for ball milled GaSb, a total conversion was achieved; however, after 90 h some residual antimony was still present in the GaSb-manually ground system. In this regard, the application of high energy ball milling was beneficial by significantly cutting down the reaction time.

The proportion of the two polytypes of GaN depended strongly on temperature/time conditions as well as on the way the precursor was ground. For 900 °C and manual grinding, the longer reaction time resulted in increased quantities of the stable h-GaN with average crystallite sizes of *ca.* 30 nm, *i.e.*, around 77% after 90 h and 92% after 170 h. This polytype was characteristic of some preferential growth as evidenced by the different values of the crystallite sizes along the selected crystallographic axes ($D(010) = 41$ nm, $D(002) = 32$ nm, $D(011) = 25$ nm). Increasing the temperature to 1000 °C, 36 h, afforded 88% of h-GaN. Interestingly, the application of ball milling resulted in the comparable quantities of h-GaN, 66–68%, independent of the conditions. This was consistent with the high energy ball milling markedly impacting the nitridation/recrystallization phenomena observed in the system. The average crystallite sizes of c-GaN were in the range of 11–14 nm, distinctly smaller than those found for h-GaN.

An additional evidence for the synthesis of GaN came from the FT-IR spectra. Typical spectra for the products are shown in Fig. 4, specifically, for the powders from 900 °C, 170 h. A band at 570–580 cm^{-1} is in the region typical for Ga–N stretches in GaN. A low intensity broad band at *ca.* 3450 cm^{-1} is an experimental artifact due to some water absorbed during the KBr pellet preparation. Moreover, a curved baseline in the range 800–4000 cm^{-1} results from no specific light scattering/absorption in the opaque pellets containing grey-yellow GaN.

The UV-vis spectra for all the product powders also supported the presence of gallium nitride. The optical spectra (absorbance *vs.* wavelength) for a selected set of 1000 °C, 36 h-
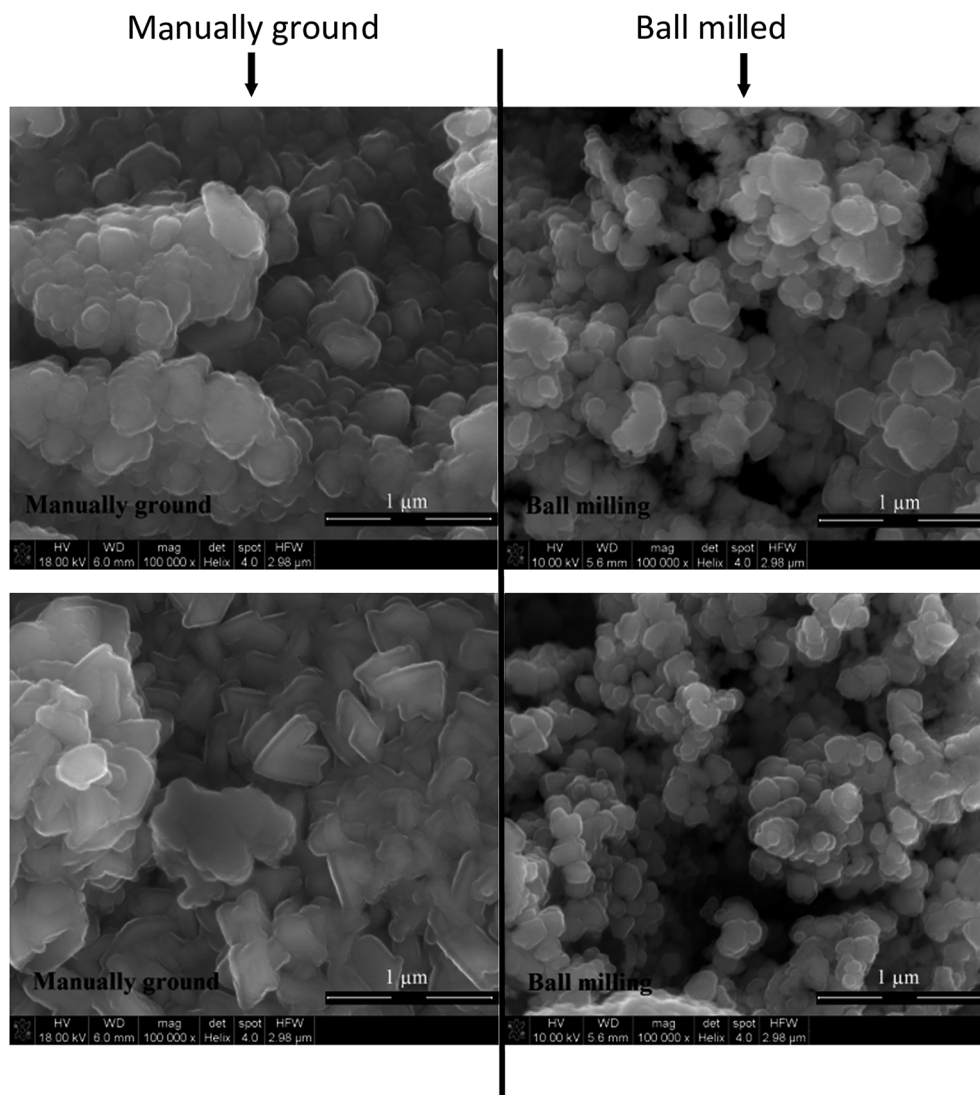
Fig. 2 SEM images of GaN nanopowders made at: top row – 900 °C, 170 h; bottom row – 1000 °C, 36 h. In both rows: left – manually ground precursor, right – ball milled precursor.

nitrided samples are shown in Fig. 5 together with the Kubelka–Munk transformations, the latter enabling calculations of specific electronic transitions (Table 2). In this regard, the energy bandgap of the GaSb substrate is 0.726 eV and corresponds to a bandgap transition at 1707 nm, which is beyond the UV-vis range. For gallium nitride materials, E_{g1} at 3.02–3.10 eV corresponds to band tail transitions linked to various impurities, disorder and defects and E_{g2} is related to the material's energy bandgap.[16] It is interesting to note that for bulk h-GaN, the bandgap transitions are expected at around 3.4 eV, whereas for c-GaN at around 3.2 eV. Given the mixture of polytypes in the powders, one tentatively assigns the E_{g2} values of 3.19–3.27 eV to c-GaN. The E_{g2} values for hexagonal gallium nitride could not be unequivocally fitted in the rather noisy parts of the spectra. However, the regions shown within the ovals in Fig. 5 could be fitted with the dotted tangent lines that consistently intersect the energy coordinate at ca. 3.4 eV, which is characteristic of h-GaN (Table 2, values in parentheses). This

would be a rare piece of evidence from standard UV-vis determinations for the mixture of the GaN polytypes in bulk powders. It is worth mentioning that the GaN average crystallite sizes are larger than 3–11 nm, the values quoted for the Bohr radius of GaN[17] and therefore, no blue shift effect for E_{g2} is expected in the current case.

A further insight into the structural details of the samples was gained from the solid state ^{71}Ga MAS NMR. The spectra for the product GaN nanopowders are shown in Fig. 6 and the peak positions estimated by best-fit curve deconvolution are collected in Table 3. In no case, a resonance at −50 ppm for GaSb was detected supporting its complete conversion to GaN. From our earlier NMR studies on a range of GaN nanopowders, we concluded that a hexagonal GaN material may have two distinct gallium resonances, i.e., at ca. 325–330 ppm and ca. 415–440 ppm.[5h,18] The former peak is relatively sharp and corresponds to good crystallinity and uniformity in the short range structural order in well crystallized h-GaN. The latter peak is quite
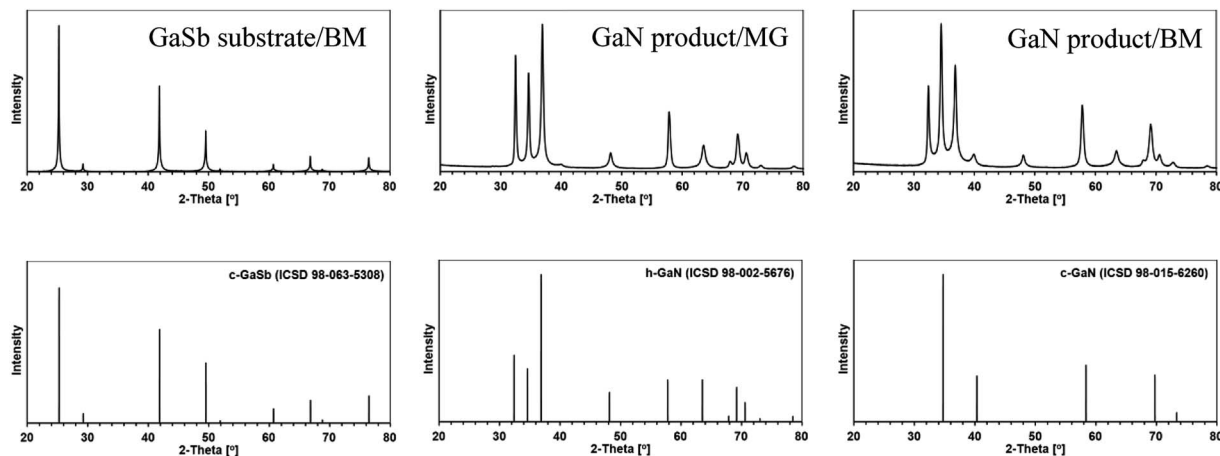
Fig. 3 XRD patterns of the products obtained from the nitridation of powdered GaSb with ammonia at 900 °C, 170 h: top left – GaSb substrate/BM, top middle – GaN product from manually ground GaSb, top right – GaN product from ball milled GaSb. MG – manually ground, BM – ball milled. The bar charts in the bottom row are for cubic GaSb (ICSD 98-063-5308) – bottom left, hexagonal h-GaN (ICSD 98-002-5676) – bottom middle and cubic c-GaN (ICSD 98-015-6260) – bottom right.

Table 1 The amounts and average crystallite sizes of the GaN polytypes (nd – not determined)

Nitridation	Grinding	h-GaN amount/av. size	c-GaN amount/av. size	Sb amount
900 °C, 90 h	Manual	77.4%/30 nm	22.2%/14 nm	0.4%
	Ball milling	66%/23 nm	34%/14 nm	—
900 °C, 170 h	Manual	92%/33 nm	8%/nd	—
	Ball milling	67%/25 nm	33%/12 nm	—
1000 °C, 36 h	Manual	88%/33 nm	12%/12 nm	—
	Ball milling	68%/24 nm	32%/11 nm	—

symmetrical and unusually broadened. From scarce and controversial literature data on its interpretation, the lower field broader peak has been assigned by some researchers either, in what appears a rather confusing way, to a postulated non-stoichiometric N-deficient phase GaN_{1-x} $(0 < x < 1)$[19] or, alternatively, in what appears to us the well-substantiated reports, to a Knight shift due to the presence of conduction electrons in the semiconductor.[20] In our studies, we observed growing intensities for the lower field peak at the expense of the higher field peak for GaN nanopowders that were subjected to recrystallization/crystal growth by annealing at increased temperatures, whereas by comparison, no such phenomenon was detected upon heating well crystalline HVPE-grown hexagonal GaN. In our opinion, the temperature-induced nanopowder recrystallization although results by XRD criteria in better crystallinity may, at the same time, introduce specific crystal defects, including native N-defect formation and/or impurity oxygen incorporation into the crystal lattice of GaN. The interpretation of the NMR spectra is even more complex if two GaN polytypes are present. It was tentatively proposed by us that a similar set of two resonances as for h-GaN could be adequately assigned to c-GaN,[5h] i.e., at 350–360 ppm and ca. 420–480 ppm. In Fig. 6, clear shoulders at 350–360 ppm on the sharp peaks can be seen of which the deconvolution-derived positions are included in Table 3. Such deconvolution could not, however, be reasonably applied to the symmetrical low field

broad peak. This could mean that the c-GaN component in it is either absent/in small quantities (only well crystalline c-GaN is present) or the peak intensities for the two polytypes add adventitiously. In such a case, the position of the broad peak in the range of ca. 420–480 ppm may be a rough estimate of the quantity of a selected peak's component.

For the manually ground GaSb-derived nanopowders (Fig. 6, left panel), they all show prevailing quantities of h-GaN, including significant proportions of the "defected" component, which is consistent with the XRD data (Table 1). Among them, the 900 °C, 170 h-powder is characteristic of the highest proportion of the well crystalline component of this type as judged from a comparison of the peak intensities in the 330 ppm range. Moreover, the corresponding low field peak of small intensity at 423 ppm supports a smaller quantity of the "defected" component. Interestingly, increasing the nitridation time from 90 to 170 h results in an increased proportion of the well crystalline component of h-GaN. This is contrary to what we observed in our previous NMR study on similar GaN nanopowders wherein annealing at temperatures higher than the nitridation temperature caused an opposite phenomenon, i.e., the relative amount of the well crystalline component decreased.[5h] The answer to this apparent ambiguity possibly lies in the different annealing conditions applied this time wherein the temperature was constant and the variable was time. In such a case, the extension of annealing time results in the overall
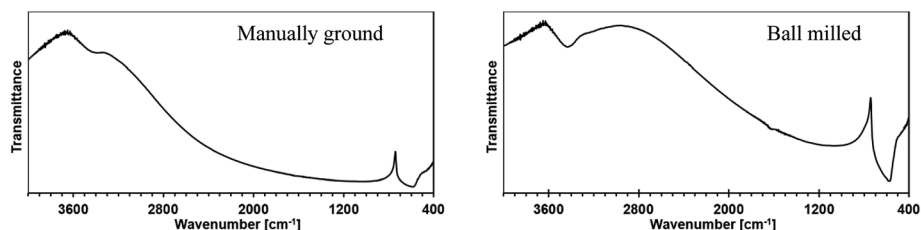
Fig. 4 FT-IR spectra of the products obtained from the nitridation of powdered GaSb with ammonia at 900 °C, 170 h: left – manually ground, right – ball milled.
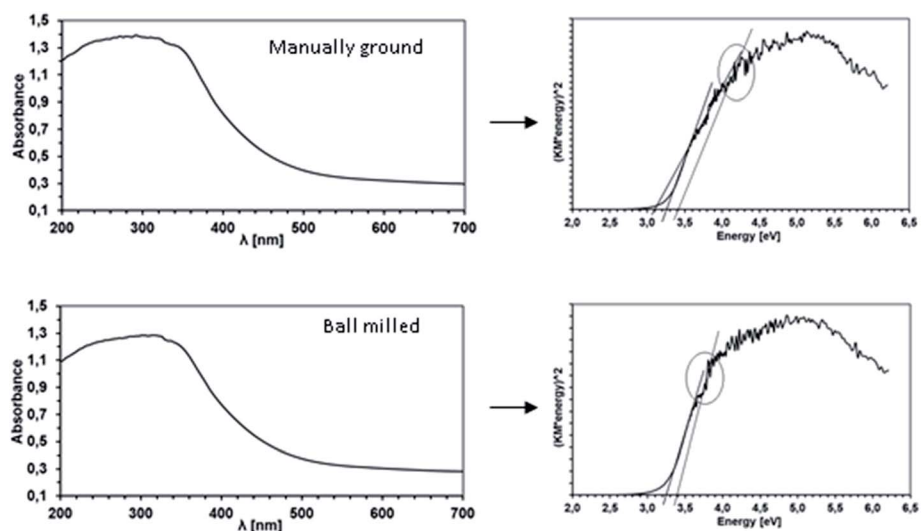

Fig. 5 Examples of the UV-vis spectra of GaN obtained from the nitridation of ground GaSb, 1000 °C, 36 h: top row – manually ground, bottom row – ball milled. The left panel shows the absorbance spectra, whereas the right panel includes the derived Kubelka−Munk functions.

higher quantity of h-GaN with increased proportions of the well crystalline component and the latter, likely, formed from the metastable c-GaN to stable h-GaN transformation, whereas the h-GaN grain recrystallization stabilizes at a temperature-determined level. Such an explanation makes the XRD and NMR data consistent.

When analyzing the ball milled GaSb-derived sample data, one notices quite similar properties in their NMR spectra with the relatively enhanced quantities of the c-GaN polytype. This is very much in accordance with the relevant XRD data. When compared with manual grinding, ball milling results not only in higher proportions of c-GaN but also in a better crystallinity of the h-GaN polytype. Increased nitridation temperatures for this

pool of nanopowders are reflected in a relatively moderate increase in the "defected" component in the spectra. Moreover, the application of ball milling results in GaN nanopowders that are more homogeneous and of better crystallinity supporting the essential role that the GaSb grain size characteristics played in nitridation which, keeping other things in proportion, conceals significantly the impact of temperature and time.

Raman spectroscopy provided yet another insight into the structural properties of the nanopowders as the method is sensitive to chemical composition (purity), crystalline polytypes and lattice defects/vacancies. The micro-Raman spectra are shown in Fig. 7 and the major peaks are listed in Table 4. The spectra were subjected to best-fitting deconvolution that eventually yielded the peaks positions. In some cases of severe peak overlapping coupled with peak low intensities, e.g., in the range 500–600 cm^{-1} or above 700 cm^{-1}, the deconvolution might not have substantiated the lowest intensity and broad peaks that still could be present. No spectrum contains the peaks for potentially unconverted cubic GaSb,[21] i.e., 228 cm^{-1} (TO mode) and 238 cm^{-1} (LO mode), which is consistent with efficient nitridation.

A striking feature of all the spectra is that the highest intensity peak is at ca. 150 cm^{-1} that is assigned to the E_2(low) phonon mode in GaN,[22a–d] which is rather uncommon among

Table 2 The UV-vis derived E_g values of the GaN nanopowders

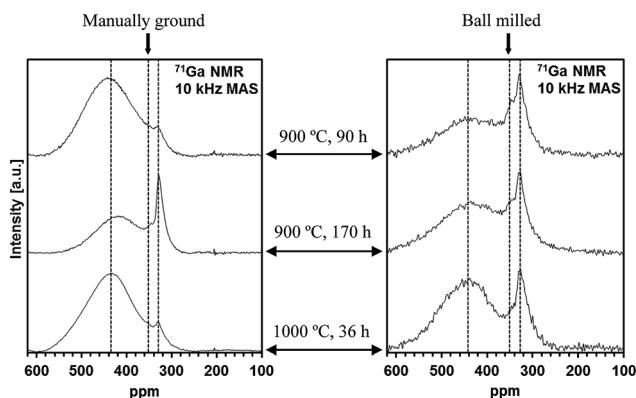| Nitridation	Grinding	E_{g1} [eV]	E_{g2} [eV]
900 °C, 90 h	Manual	—	3.19
	Ball milling	—	3.27
900 °C, 170 h	Manual	3.03	3.25
	Ball milling	3.02	3.27
1000 °C, 36 h	Manual	3.10	3.27, (3.40)
	Ball milling	—	3.25, (3.40)

Fig. 6 Solid state ^{71}Ga MAS NMR spectra of GaN obtained from the nitridation of ground GaSb: left panel – manually ground, right panel – ball milled. The reaction temperatures and times are shown next to the spectra.

Table 3 ^{71}Ga MAS NMR peak positions (n/d – not determined)

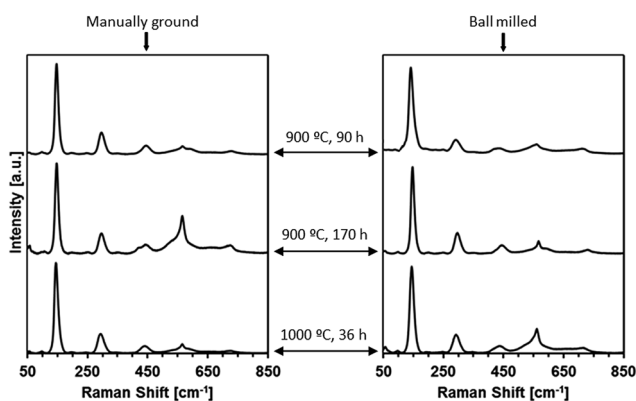| Nitridation	Grinding	High field peak [ppm]		Low field peak [ppm]	
		h-GaN	c-GaN	h-GaN	c-GaN
900 °C, 90 h	Manual	330	353	445	n/d
	Ball milling	331	353	439	n/d
900 °C, 170 h	Manual	331	353	423	n/d
	Ball milling	331	353	434	n/d
1000 °C, 36 h	Manual	336	352	439	n/d
	Ball milling	331	349	445	n/d

Fig. 7 Raman spectra of the GaN obtained from the nitridation of ground GaSb: left panel – manually ground, right panel – ball milled. The reaction temperatures and times are shown next to the spectra.

various gallium nitride materials. This peak is, in some cases, asymmetrical and results in two deconvoluted components. In this regard, the sharpness and high intensity of the E_2(low) peak in related wurzitic ZnO films was attributed to improved crystal quality,[23] in our case well agreeing with the relevant XRD data. The E_2(low) phonon mode is specific for hexagonal GaN and the presence of two peaks in this range can be related to two peaks

for the h-GaN component in the gallium NMR spectra. One of the two well crystalline h-GaN varieties may be stoichiometric (sharper higher field NMR peak), whereas the other one may be N-deficient/N-defected (broader lower field NMR peak), speaking in terms of explanations offered by the NMR determinations (*vide supra*). Moreover, an unexpected feature in all the spectra is the presence of two medium intensity peaks at *ca.* 300 cm^{-1} and *ca.* 440 cm^{-1}, some of which are deconvoluted into two components. Literature interpretation of the 300 cm^{-1} peak has involved either a lower symmetry activation of the otherwise silent B_1(low) mode in h-GaN[22e,f] or its assignment to the host lattice vibrational states,[22g] whereas the peak around 440 cm^{-1} has been proposed to result from nitrogen vacancy-related defects.[22g] It is appropriate to mention here that another peak at 659–671 cm^{-1} was also attributed to nitrogen defects,[22a,d,g] although a B_1(high) activated mode was proposed as well.[22f] In general, the presence of the N-defect related peaks conforms well with the ^{71}Ga MAS NMR data and the N-deficient phase peaks there.

The Raman spectra also contained all the other allowed peaks for both GaN polytypes, *i.e.*, for h-GaN – A_1(TO), A_1(LO), E_1(LO), E_1(TO), E_2(high) and for c-GaN – TO and LO modes. However, unfortunately, many of them lie very close to others and may, therefore, merge so their assignment may be rather ambiguous. This is the situation in the region of *ca.* 530–600 cm^{-1} wherein four peaks are expected and above 700 cm^{-1} wherein three peaks can occur for the two polytypes, as shown in Table 4. That is why in the region of *ca.* 530–600 cm^{-1}, the positions of the deconvoluted peaks are included without a strict assignment of each phonon mode, whereas generally they confirm the presence of two GaN polytypes. In the region above 700 cm^{-1}, there is only one deconvoluted peak but given the peak's small intensity and broadness other components may be just be unresolved. In this regard, the A_1(LO) mode has been reported to be absent in GaN samples with high free-carrier concentrations.[22g] In summary of this aspect, the Raman spectra for all samples were of very good quality and all major modes for the two GaN polytypes were resolved with a low background noise in the entire spectral range. This was consistent with high purity and very good crystallinity of the GaN.

From the discussion of all the characterization data, it is evident that only a combination of the various methods, such as XRD diffractometry and UV-vis, Raman and NMR spectroscopy, can provide a comprehensive description of the GaN nano-powder structures with unquestionably diverse intrinsic properties. In this regard, the application of high resolution TEM may in favorable cases be extremely useful, especially, to visualize cases of intra-growth of regular and hexagonal domains within a nanograin but such an approach was outside the scope of this project.

3.3. Pathways in the ammonolysis of GaSb

The overall picture that emerges from this study involves a specific reactivity pattern in the ammonolysis of GaSb, which includes two concurrent pathways – one which leads to

Table 4 Positions of the deconvoluted peaks in the micro-Raman scattering determinations of the GaN nanopowders. The two symmetry allowed modes for c-GaN are shown in italics

| Mode assignment	Raman shift [cm^{-1}]					
	From manually ground precursor			From ball milled precursor		
	900 °C, 90 h	900 °C, 170 h	1000 °C, 36 h	900 °C, 90 h	900 °C, 170 h	1000 °C, 36 h
E$_2$(low)[22a–d]	147	148	145	141	147	144
			153	151	150	156
B$_1$(low) silent[22e,f], host lattice vibrations[22g]	297	297	292	293	296	292
			309		311	308
Nitrogen vacancies[22g]	445	418	440	433	421	435
		444			445	
A$_1$(TO), E$_1$(LO), E$_2$(high)[22a–d], *TO(c-GaN)*[22b,d]	541	539	545	545	549	526
	—	552	554	—	555	549
	565	566	565	560	567	561
	589	594	585	590	593	574
B$_1$(high) silent[22f], nitrogen vacancies[22a,d,g]	668	671	661	668	659	667
A$_1$(LO), E$_1$(TO)[22a], *LO(c-GaN)*[22b,d]	727	723	725	714	729	715
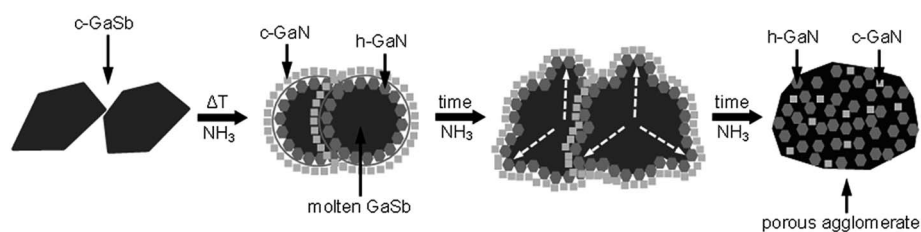
Fig. 8 Ammonolytical nitridation of microcrystalline particles of c-GaSb to mixtures of nanocrystalline particles of h-GaN and c-GaN.

metastable cubic GaN likely *via* formation of transient cubic GaSb$_x$N$_y$ species and another which results in stable hexagonal GaN *via* ammonolysis of molten/decomposed GaSb. An outstanding problem beyond the scope of this study is the temperature dependent dynamics of c-GaN to h-GaN transformation in bulk powders, which has not yet been fully addressed in the literature. Fig. 8 graphically depicts the proposed sequence of the major events that are supported by the experimental data.

In the initial nitridation stages, solid layers of short lived/ unstable c-GaSb$_x$N$_y$ are proposed to form first on the c-GaSb particle surfaces, which efficiently undergo further ammonolysis towards metastable c-GaN. This stage is topochemically controlled and decides the final relative amounts of the cubic polytype. Simultaneously, upon reaching the melting point of GaSb at 712 °C, the particle core melts and diffusion controlled ammonolysis of molten GaSb produces the stable h-GaN in admixture with Sb. The in and out gas/vapor fluxes cause, eventually, particle deterioration and mixing of the two GaN polytypes into agglomerates. Increasing the reaction time at 900 °C from 90 to 170 h results in increased proportions of the stable h-GaN, possibly, *via* a thermodynamically favourable and relatively slow c-GaN to h-GaN transformation. Eventually, for manually ground GaSb, the mixtures of both GaN polytypes with predominant h-GaN are produced and the latter amounts

to 77%–92%, depending on the nitridation temperature and time. Deeper grinding of GaSb by high energy ball milling shortens the effective reaction time and provides nanopowders with surprisingly stable c-Gan to h-GaN proportions in all products, *i.e.*, with h-GaN in the range of 66%–68% suppressing greatly the time/temperature effect. It appears that the overall long nitridation times in the studied temperature range, especially at 900 °C, are determined to a great extent by the rather slow removal of the antimony by-product vapors from the system.

4. Conclusions

The ammonolytical nitridation of GaSb constitutes a new convenient way for a one-stage preparation of h-GaN-rich nanopowders of high purity, very good crystallinity and controlled c-GaN to h-GaN proportions under relatively conservative conditions. The concurrent formation of the metastable cubic GaN is consistent with the topochemistry playing a significant role in the nitridation of cubic GaSb, in which it competes with the thermodynamically favourable pathways leading to stable hexagonal GaN. The formation of the latter results from the ammonolysis of molten GaSb and/or liquid Ga produced from the thermally induced decomposition of GaSb, with both events being virtually unavoidable at

practical reaction temperatures, whereas the former appears to be a function of the rate of ammonolysis of the solid GaSb. From this point of view, controlling these factors is a key to an engineered synthesis of GaN polytypes. In this regard, one of the essential factors is the GaSb substrate particle size/particle surface area, which is determined by the grinding method.

A more comprehensive description of the formation and stability of both GaN polytypes in the *in statu nascendi* prepared nanopowders requires additional studies on the c-GaN *vs.* h-GaN equilibria as a function of crucial experimental parameters such as temperature, time, and gas atmosphere. An intriguing question of a frequently interrelated intra-growth of the cubic and hexagonal domains in a nitride nanograin has also to be addressed. Such studies are planned in our laboratory in the near future.

Acknowledgements

References

1 (*a*) I. Akasaki, *Angew. Chem., Int. Ed.*, 2015, **54**, 7750–7763; (*b*) H. Amano, *Angew. Chem., Int. Ed.*, 2015, **54**, 7764–7769; (*c*) S. Nakamura, *Angew. Chem., Int. Ed.*, 2015, **54**, 7770–7788; (*d*) S. S. Khludkov, I. A. Prudaev and O. P. Tolbanov, *Russ. Phys. J.*, 2013, **55**, 903–909; (*e*) M. S. Kang, C. H. Lee, J. B. Park, H. Yoo and G. C. Yi, *Nano Energy*, 2012, **1**, 391–400.

2 (*a*) T. Hashimoto, E. Letts and S. Hoff, *Sens. Mater.*, 2013, **25**, 155–164; (*b*) R. Dwilinski, R. Doradzinski, J. Garczynski, L. Sierzputowski, R. Kucharski, M. Zajac, M. Rudzinski, R. Kudrawiec, W. Strupinski and J. Misiewicz, *Phys. Status Solidi A*, 2011, **208**, 1489–1493; (*c*) M. Bockowski, P. Strak, I. Grzegory and S. Porowski, *Technology of gallium nitride crystal growth*, Book Series: Springer Series in Materials Science, 2010, vol. 133, pp. 207–234; (*d*) V. Avrutin, D. Silversmith, Y. Mori, F. Kawamura, Y. Kitaoka and H. Morkoc, *Proc. IEEE*, 2010, **98**, 1302–1315.

3 (*a*) M. A. Malik, M. Afzaal and P. O'Brien, *Chem. Rev.*, 2010, **110**, 4417–4446; (*b*) B. Mazumder and A. L. Hector, *J. Mater. Chem.*, 2009, **19**, 4673–4686; (*c*) C. N. R. Rao, C. R. C. Vivekchand, K. Biswas and A. Govindaraj, *Dalton Trans.*, 2007, 3728–3749; (*d*) J. A. Jegier, S. McKernan, A. P. Purdy and W. L. Gladfelter, *Chem. Mater.*, 2000, **12**, 1003–1010; (*e*) R. L. Wells and W. L. Gladfelter, *J. Cluster Sci.*, 1997, **8**(2), 17–238.

4 R. L. Wells and J. F. Janik, *Eur. J. Solid State Inorg. Chem.*, 1996, **33**, 1079–1090.

5 (*a*) J. F. Janik and R. L. Wells, *Chem. Mater.*, 1996, **8**, 2708–2711; (*b*) J. L. Coffer, M. A. Johnson, L. Zhang, R. L. Wells and J. F. Janik, *Chem. Mater.*, 1997, **9**, 2671–2673; (*c*) J. F. Janik, R. L. Wells, J. L. Coffer, J. V. St. John, W. T. Pennington and G. L. Shimek, *Chem. Mater.*, 1998, **10**, 1613–1622; (*d*) J. L. Coffer, T. W. Zerda, R. Appel, R. L. Wells and J. F. Janik, *Chem. Mater.*, 1999, **11**, 20–22; (*e*) L. Czepirski, J. F. Janik, E. Komorowska-Czepirska and

R. L. Wells, *Adsorpt. Sci. Technol.*, 2002, **20**, 723–728; (*f*) R. L. Jouet, A. P. Purdy, R. L. Wells and J. F. Janik, *J. Cluster Sci.*, 2002, **13**, 469–486; (*g*) J. F. Janik, *Powder Technol.*, 2005, **152**, 118–126; (*h*) M. Drygas, Z. Olejniczak, E. Grzanka, M. M. Bucko, R. T. Paine and J. F. Janik, *Chem. Mater.*, 2008, **20**, 6816–6828; (*i*) M. Drygas and J. F. Janik, *Mater. Chem. Phys.*, 2012, **133**, 932–940.

6 J. F. Janik and R. L. Wells, *Inorg. Chem.*, 1997, **36**, 4135–4137.

7 (*a*) G. L. Wood, E. A. Pruss and R. T. Paine, *Chem. Mater.*, 2001, **13**, 12–14; (*b*) J. F. Janik, M. Drygas, S. Stelmakh, E. Grzanka, B. Palosz and R. T. Paine, *Phys. Status Solidi A*, 2006, **203**, 1301–1306.

8 (*a*) S. Stelmakh, A. Swiderska-Sroda, G. Kalisz, S. Gierlotka, E. Grzanka, B. Palosz, M. Drygas, J. F. Janik and R. T. Paine, *Proceedings of the International Conference on Nanoscience and Technology, Basel, Switzerland, July 30-Aug 4, 2006*, Institute of Physics Publishing, Philadelphia, PA, 2006; (*b*) E. Grzanka, S. Stelmakh, S. Gierlotka, A. Swiderska-Sroda, G. Kalisz, B. Palosz, M. Drygas, J. F. Janik and R. T. Paine, *European Powder Diffraction Conference, EPDIC-10*, Geneva, Switzerland, September 1–4, 2006-*Z. Kristallogr.* 2007, **26**, MS11-P2; (*c*) J. Borysiuk, P. Caban, W. Strupinski, S. Gierlotka, S. Stelmakh and J. F. Janik, *Cryst. Res. Technol.*, 2007, **42**, 1291–1296; (*d*) Polish patent No. P-378458: way to make sintered gallium nitride GaN; patent issued as published in *Wiadomości Urzędu Patentowego* (News of the Polish Patent Office), No. 2/2012, Feb. 29, 2012.

9 (*a*) A. Addamiano, *J. Electrochem. Soc.*, 1961, **108**, 1072; (*b*) W. S. Jung, O. H. Han and S. A. Chae, *Mater. Chem. Phys.*, 2006, **100**, 199–202; (*c*) M. Drygas, M. M. Bucko, E. Grzanka and J. F. Janik, *Curr. Nanosci.*, 2013, **9**, 173–182.

10 J. W. Hwang, J. P. Campbell, J. Kozubowski, S. A. Hanson, J. F. Evans and W. L. Gladfelter, *Chem. Mater.*, 1995, **7**, 517–525.

11 M. A. Todd, G. Bandari and T. H. Baum, *Chem. Mater.*, 1991, **11**, 547–551.

12 J. Deslippe and S. G. Louie, *Ab initio* theories of the structural, electronic, and optical properties of semiconductors: bulk crystals to nanostructures, in *Comprehensive Semiconductor Science and Technology*, ed. P. Bhattacharya, R. Fornari and H. Kamimura, Elsevier, 2011, p. 51.

13 (*a*) A. Mondal, T. D. Das, N. Halder, S. Dhar and J. Kumar, *J. Cryst. Growth*, 2001, **297**, 4–6; (*b*) V. L. Berkovits, A. B. Gordeeva, T. V. L'vova and V. P. Ulin, *Semiconductors*, 2012, **46**, 1432–1436; (*c*) D. Wang, S. P. Svensson, L. Shterengas, G. Belenky, C. S. Kim, I. Vurgaftman and J. R. Meyer, *J. Appl. Phys.*, 2009, **105**, 014904; (*d*) L. Buckle, B. R. Bennett, S. Jollands, T. D. Veal, N. R. Wilson, B. N. Murdin, C. F. McConville and T. Ashley, *J. Cryst. Growth*, 2005, **278**, 188–192; (*e*) J. Buckeridge, D. O. Scanlon, T. D. Veal, M. J. Ashwin, A. Walsh and C. R. Catlow, *Phys. Rev. B: Condens. Matter Mater. Phys.*, 2014, **89**, 014107.

14 (*a*) C. Y. Yeh, Z. W. Lu, S. Froyen and A. Zunger, *Phys. Rev. B: Condens. Matter Mater. Phys.*, 1992, **46**, 10086–10097;

(b) A. Zoroddu, F. Bernardini, P. Ruggerone and V. Fiorentini, *Phys. Rev. B: Condens. Matter Mater. Phys.*, 2001, **64**, 045208.

15 S. Suandon, S. Sanorpim, K. Yoodee and K. Onabe, *Thin Solid Films*, 2007, **515**, 4393–4396.

16 I. Akyuz, S. Kose, F. Atay and V. Bilgin, *Semicond. Sci. Technol.*, 2006, **21**, 1620–1626.

17 (a) P. Ramvall, S. Tanaka, S. Nomura, P. Riblet and Y. Aoyagi, *Appl. Phys. Lett.*, 1998, **73**, 1104–1106; (b) X. L. Chen, J. N. Li, Y. G. Cao, Y. C. Lan, H. Li, M. He, C. Y. Wang, Z. Zhang and Z. Y. Qiao, *Adv. Mater.*, 2000, **12**, 1432–1434.

18 M. Drygas, M. M. Bucko, Z. Olejniczak, I. Grzegory and J. F. Janik, *Mater. Chem. Phys.*, 2010, **122**, 537–543.

19 (a) W. S. Jung, C. Park and S. Han, *Bull. Korean Chem. Soc.*, 2003, **24**, 1011–1013; (b) W. S. Jung, *Mater. Lett.*, 2006, **60**, 2954–2957; (c) W. S. Jung, O. H. Han and S. A. Chae, *Mater. Chem. Phys.*, 2006, **100**, 199–202; (d) B. Schwenzer, J. Hu, R. Seshadri, S. Keller, S. P. DenBaars and U. K. Mishra, *Chem. Mater.*, 2004, **16**, 5088–5095; (e) B. Schwenzer, J. Hu, Y. Wu and U. K. Mishra, *Solid State Sci.*, 2006, **8**, 1193–1201.

20 (a) J. P. Yesinowski and A. P. Purdy, *J. Am. Chem. Soc.*, 2004, **126**, 9166–9167; (b) J. P. Yesinowski and A. P. Purdy, *J. Am. Chem. Soc.*, 2006, **128**, 4952–4953; (c) J. P. Yesinowski, *Phys. Status Solidi C*, 2005, **2**, 2399–2402; (d) J. P. Yesinowski, A. P. Purdy, H. Wu, M. G. Spencer, J. Hunting and F. J. DiSalvo, *J. Am. Chem. Soc.*, 2006, **128**, 4952–4953; (e) J. P. Yesinowski, Solid-state NMR of inorganic semiconductors, in *Solid State NMR Book SeriesTopics in Current Chemistry*, ed. J. C. C. Chan, Springer, 2012, vol. 306, pp. 229–312.

21 S. V. Demishev, Y. V. Kosichkin, A. G. Lyapin, N. N. Mel'nik, D. V. Nekhaev, N. E. Sluchanko and O. A. Turok, *J. Exp. Theor. Phys.*, 1993, **77**, 329–336.

22 (a) M. Gopalakrishnan, V. Purushothaman, P. S. Venkatesh, V. Ramakrishnan and K. Jeganathan, *Mater. Res. Bull.*, 2012, **47**, 3323–3329; (b) Y. S. Wu, W. K. Chang and H. Y. Lai, *J. Cryst. Growth*, 2008, **310**, 2800–2805; (c) M. S. Kumar and J. Kumar, *Mater. Chem. Phys.*, 2002, **77**, 341–345; (d) H. Harima, *J. Phys.: Condens. Matter*, 2002, **14**, R967–R993; (e) A. Hushur, M. H. Manghnani and J. Narayan, *J. Appl. Phys.*, 2009, **106**, 054317; (f) F. J. Manjóna, B. Marí, J. Serrano and A. H. Romero, *J. Appl. Phys.*, 2005, **97**, 053516; (g) M. Katsikini, K. Papagelis, E. C. Paloura and S. Ves, *J. Appl. Phys.*, 2003, **94**, 4389–4394.

23 C. Wang, Z. Chen, Y. He, L. Li and D. Zhang, *Mater. Sci.–Pol.*, 2010, **28**(1), 153–161.